

Design Automation for Digital Microfluidic Biochips

TSUNG-YI HO^{1,a)}

Received: August 10, 2013, Released: February 14, 2014

Abstract: Microfluidic biochips are replacing the conventional biochemical analyzers, and are able to integrate on-chip all the basic functions for biochemical analysis. The “digital” microfluidic biochips (DMFBs) are manipulating liquids not as a continuous flow, but as discrete droplets on a two-dimensional array of electrodes. Basic microfluidic operations, such as mixing and dilution, are performed on the array, by routing the corresponding droplets on a series of electrodes. The challenges facing biochips are similar to those faced by microelectronics some decades ago. To meet the challenges of increasing design complexity, computer-aided-design (CAD) tools are being developed for DMFBs. This paper provides an overview of DMFBs and describes emerging CAD tools for the automated synthesis and optimization of DMFB designs, from fluidic-level synthesis and chip-level design to testing. Design automations are expected to alleviate the burden of manual optimization of bioassays, time-consuming chip designs, and costly testing and maintenance procedures. With the assistance of CAD tools, users can concentrate on the development and abstraction of nanoscale bioassays while leaving chip optimization and implementation details to CAD tools.

Keywords: cyberphysical integration, microfluidics, synthesis

1. Introduction

Microfluidic-based biochips are soon revolutionizing clinical diagnostics and many biochemical laboratory procedures due to their advantages of automation, cost reduction, portability, and efficiency [46]. Conventional technology depends on the manipulation of continuous liquid flow through microfabricated channels. However, actuation of flow is implemented with external assistance of micro-pump and micro-valve, which are complex and cumbersome. Moreover, permanently-etched channels greatly restrict the feasibility and versatility. Therefore, microfluidic research is witnessing a paradigm shift from the continuous-flow-based architecture to *droplet*-based architecture or, in particular, the *digital microfluidic biochip* (DMFB) [6], [19], [20], [29], [46].

Generally, a DMFB consists of a two-dimensional (2D) electrode array and peripheral devices such as optical detector and dispensing port, as schematically shown in Fig. 1 [19], [46]. The sample carriers, *droplets*, being miniaturized and *discretized* liquids, are controlled by underlying electrodes using electrical actuations (i.e., a principle called electrowetting-on-dielectric or EWOD) [38]. By assigning time-varying voltage values to turn on/off electrodes, droplets can be moved around the entire 2D array to perform fundamental operations (e.g., dispensing and mixing) [42]. These operations are carried out in a *reconfigurable* manner due to their flexibility in area and time domain [6]. Compared with continuous-flow-based biochips, DMFBs offer various advantages including more flexible control mechanism and higher throughput and sensitivity as well as lower sample/reagent volume consumption.

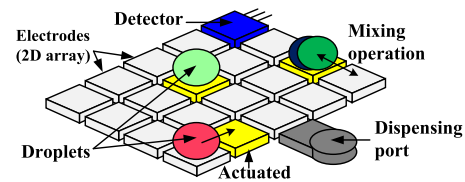


Fig. 1 The schematic view of a DMFB.

Due to these advantages, DMFBs have attracted many efforts being devoted to marketplace demands, ranging from healthcare, environmental sensing, and point-of-care-testing applications. Frost & Sullivan recently predicted a 13.5% Compound Annual Growth Rate for the Europe biochip (“lab-on-chip”) market during 2008–2015, and the market size for lab-on-chip alone (not including microarrays, biosensors, and microreactors) is expected to be over 1.6 billion in 2015 [2]. Similar growth is anticipated in other parts of the world, especially US and Japan. Continuing growth of various applications have dramatically complicated chip/system integration and design complexity [7], [19], [20], rendering traditional manual designs infeasible, especially under time-to-market constraints. Hence, it is necessary to develop high-quality computer-aided-design (CAD) tools for efficient design automation. Design automations are expected to reduce the burden associated with manual optimization of bioassays, time-consuming chip designs, and costly testing and maintenance procedures. Moreover, the assistance of CAD tools will facilitate the integration of fluidic components with a microelectronic component in next-generation system-on-chips (SOCs) [6], [7], [19], [20], [46].

In this paper, we provide a survey of recent research and emerging challenges in design and optimization for DMFBs. We show how CAD approaches can be used to automate and optimize the design of DMFBs in fluidic domain and chip (i.e., hardware)

¹ Department of Computer Science and Information Engineering, National Cheng Kung University, Tainan, Taiwan

^{a)} tyho@csie.ncku.edu.tw

domain. The goal in this paper is to give a holistic perspective on top-down system-level CAD tools, and discuss several associated combinatorial and geometric optimization problems. Having these CAD tools, users and designers will be able to describe bioassays at a high-level of abstraction. CAD tools will generate an optimized schedule of bioassay operations, a suitable chip layout for best fluidic performance, and well-planned signal connections for low-cost manufacturing process. Therefore, biochip users and designers can concentrate on innovations at the application level, leaving implementation details to CAD tools. These CAD tools will reduce human effort and enable high-volume production. The remainder of the paper is organized as follows: Section 2 reviews the typical CAD flow of DMFB that consists of fluidic-level synthesis and chip-level design. Section 3 and Section 4 discuss the related optimization problems and CAD approaches in fluidic-level synthesis and chip-level design, respectively. Section 5 presents the error recovery cyberphysical microfluidics that achieve closed-loop and sensor feedback-driven biochip operation under program control.

Section 6 describes the design challenges and several open problems that remain to be tackled in the future. Finally, conclusion is drawn in Section 7.

2. CAD Flow of DMFBs

A regular CAD flow of DMFBs consists of two stages, *fluidic-level synthesis* and *chip-level design* [19], as illustrated in Fig. 2. Fluidic-level synthesis describes an automated scheduling of assays and a generation of a mapping of assay operations to resources in a time-multiplexed manner. Fluidic-level synthesis is divided into two major phases, referred to as architectural-level synthesis (i.e., high-level synthesis) and geometry-level synthesis (i.e., physical design) [43], [44], [46]. Optimizations here are guaranteeing high-performance fluidic behaviors as well as a suitable chip layout. On the other hand, the goal in chip-level design is determining the control-signal plan and electrical connections for the electrodes to execute the synthesized result. Chip-level design consists of two steps of electrode addressing followed by wire routing [19], [24]. This design stage is receiving increasing attention in recent years as it dominates the manufacturing complexity and fabrication cost of a DMFB.

In the following sections, we provide a progression of the re-

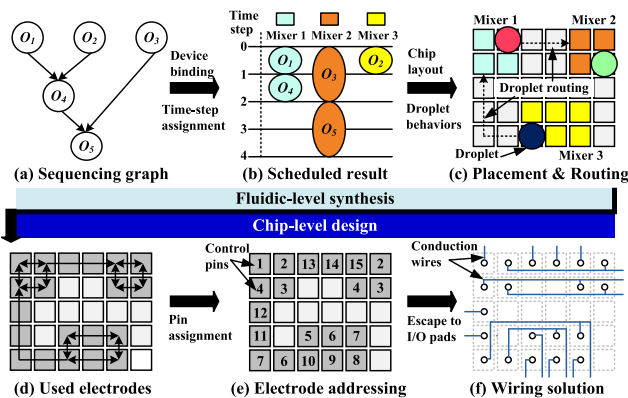


Fig. 2 Regular CAD flow of DMFBs consists of two stages of fluidic-level synthesis followed by chip-level design.

lated CAD problems and research on fluidic-level synthesis and chip-level design, respectively.

3. Fluidic-Level Synthesis

In this section, we discuss automated fluidic-level synthesis.

Hierarchical and cell-based design techniques from modern very-large-scale-integration (VLSI) automation has been utilized for architectural-level synthesis and geometry-level synthesis.

3.1 Architectural-Level Synthesis

An assay is typically abstracted as a model of sequencing graph (see Fig. 2 (a)). The sequencing graph is directed, acyclic and polar (i.e., there is a source node without predecessors and a sink node without successors). Each node represents a specific assay operation (e.g., mixing, generation, and detection), while a directed edge indicates the dependency between two operations.

In architectural-level synthesis, both the resource-binding problem and the scheduling problem are addressed to generate a structural view of a biochip design. As analogous to high-level synthesis for integrated circuits, resource binding determines a mapping from assay operations to available functional resources. There may be several types of resources for any given assay operation. For example, a 2×2 mixer and a 2×3 mixer can be used for a mixing operation but with different mixing times. A resource binding procedure is applied to determine the selections with a minimized assay execution time. Once resource binding is carried out, the execution time for each assay operation can be roughly determined. In other words, scheduling of the start times and stop times of all assay operations is determined, subject to the precedence constraints by the given sequencing graph, as illustrated in Fig. 2 (b).

Several algorithms, such as tabu-search based synthesis [35] and ILP (integer-linear-programming) based synthesis [43], are proposed to handle the basic architectural-level synthesis of DMFBs. Also, a unified high-level synthesis and module placement methodology has been proposed in Ref. [44], where the focus has been on deriving an implementation that can tolerate faulty cells in the biochip array. Their algorithm was modified in Ref. [53] to include droplet-routing-aware physical design decisions.

Different from traditional module-based operation execution that all cells inside the module are considered occupied, an alternative routing-based operation execution is proposed [36]. In Ref. [36], mixing process is performed by routing, i.e., an operation can be executed anywhere on the array, unconstrained by a rectangular shape representing a virtual module. Compared to traditional module-based mixing operation in Fig. 3 (a), this characteristic of the mixing operation is shown in Fig. 3 (b), where the droplet is routed freely on a sequence of electrodes, according to the shown route.

3.2 Geometry-Level Synthesis

A key problem in the geometry-level (i.e., physical-level) synthesis of DMFBs is the placement of fluidic modules such as different types of mixers and detection units. The major goal of the placement is to find the actual locations of different flu-

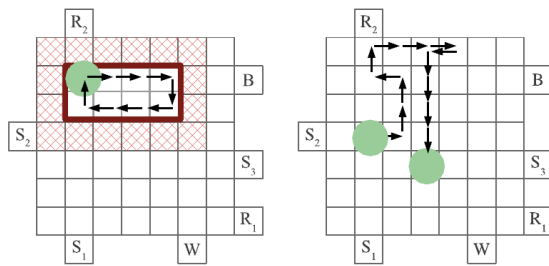


Fig. 3 (a) Module-based operation execution (b) Routing-based operation execution.

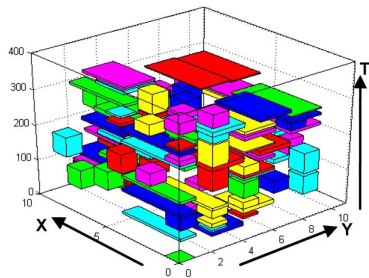


Fig. 4 3D packing diagram of a placement result.

idic modules corresponding to different time intervals. Since DMFBs enable dynamic reconfiguration of the microfluidic array during run-time, they allow the placement of different modules on the same location during different time intervals [45], [47]. Therefore, the placement of modules can be modeled as a three-dimensional (3D) packing problem. Each fluidic module represents a 3D box, the base of which denotes the rectangular area of the module and the height denotes the time span of its execution, see **Fig. 4** for an example.

The most important optimization objective of the placement problem is the minimization of chip area. Since solutions of the placement problem can provide the designers with guidelines on the chip size to be manufactured, area minimization frees up more unit cells for other fluidic functions such as sample preparation and collection. During the placement, some performance constraints including the upper limit on assay completion time and maximum allowable chip array should be satisfied, in order that the system reliability and integrity inherent from the architectural-level synthesis can be well-maintained. Besides, since the increasing assay density and area of DMFBs may potentially reduce yield, a critical issue of *fault tolerance* is also considered to avoid defective cells due to fabrication. Since we need time to ramp up the yield of DMFBs, it is desirable to perform a bioassay on a DMFB with the existence of defects (i.e., fabrication faults). How to integrate the defect tolerant issue into the placement problem with correct fluidic functions has become an important issue. To handle such a problem, some algorithms, such as simulated-annealing (SA)-based optimization [44], [47] and T-tree-based placement formulation [56], are presented in recent years. Besides, a work in Ref. [4] further considers the control-path based synthesis with placement to minimize the operation variability. Different from SA method which is time consuming and does not guarantee to obtain an optimal solution, a 3D Deferred Decision Making (3D-DDM) technique to enumerate only possible placement solutions is proposed [10]. Moreover,

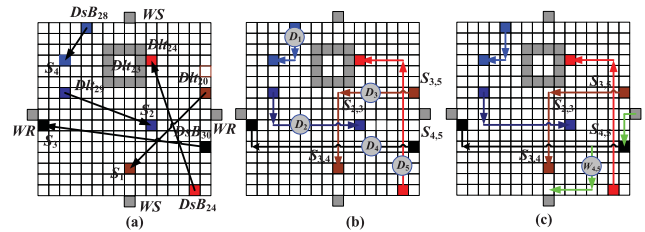


Fig. 5 Synchronization of washing operations and droplet routing [60]. (a) A droplet routing result. (b) Washing operations on contaminated spot $S_{4,5}$.

in order to speed up the computation time, it also proposes a novel technique that prunes most redundant computations without affecting solution quality.

Droplet routing on DMFBs is a key design issue in the physical-level synthesis, which schedules the movement of each droplet in a time-multiplexed manner. The major goal of droplet routing is constructing the connections between modules, and between modules and I/O ports (i.e., on-chip reservoirs) within different time intervals. This physical synthesis is one of the most critical design challenges due to design complexity as well as large impacts on correct assay performance. Since a microfluidic array is reconfigured dynamically at run-time, the inherent reconfigurability allows different droplet routes to share cells on the microfluidic array during different time intervals. Besides, a series of 2D placement configurations of fluidic modules in different time intervals are obtained in the placement stage. Therefore, droplet routing is decomposed into a series of *sub-problems*, which establishes the connections for pre-placed fluidic modules between successive sub-problems. We can thus obtain a complete droplet routing solution by solving these sub-problems sequentially. In this sense, the routes on the microfluidic array can be viewed as *virtual routes* in a 3D manner, which make the droplet routing problem different from the classical wire routing in VLSI designs [48]. Systematic droplet routing methods have therefore been developed to minimize the number of cells used for droplet routing for better fault, while satisfying constraints imposed by performance goals and fluidic properties [21], [23], [48], [57], [62].

Cross-contamination is likely to occur when multiple droplet routes intersect or overlap with each other. At the intersection site of two droplet routes, a droplet that arrives at a later clock cycle can be contaminated by the residue left behind by another droplet that passed through at an earlier clock cycle. To avoid assay execution error, washing operations (i.e., wash-droplet routing) are introduced to clean the contamination left on the surface [22], [58], [60]. In Ref. [58], a disjoint route algorithm is applied to avoid the overlap between different routes, with insertions of washing operations between successive droplet routing subproblems. In Ref. [22], a network-flow based algorithm is utilized to formulate simultaneous droplet routing and washing operations. The work in Ref. [60], synchronizes wash-droplet routing with sample/reagent droplet-routing steps by controlling the arrival order of droplets at cross-contamination sites. **Figure 5** shows a synchronization result of washing operations.

Recently, the work in Ref. [31] considers the cross-

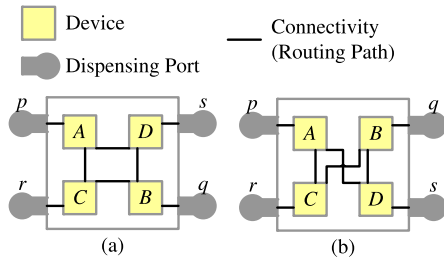


Fig. 6 Different placement topology leads to different numbers of crossing routing paths [31]. (a) Zero crossing routing path. (b) One crossing routing path.

contamination avoidance in earlier design stage of placement. As illustrate in **Fig. 6**, it generates a placement topology with a minimized number of crossing routing paths by using a bipartite matching formulation. Therefore, the efforts spent on routing wash droplets can be minimized.

4. Chip-Level Design

In this section, we discuss chip-level design, which consists of electrode addressing and wire routing^{*1}, as shown in Fig. 2 (d)–(f). We first show the EWOD actuator of digital microfluidics and then discuss the electrode addressing and wire routing.

4.1 Architecture and Design Model of EWOD Chips

In performing various fluidic-handling functions, a primary issue is the manipulation of droplets. Although droplets can be controlled on many driving platforms [46], the EWOD chips, also referred to as EWOD actuators, have received much more attention due to their high accuracy and efficiency, and simple fabrication [17]. The EWOD chip generates electric potential by actuating electrodes to change the wettability of droplets, such that droplets can be shaped and driven along the active electrodes [38], [42]. To induce enough change of wettability for droplet motion, the voltage value applied to electrodes must exceed a threshold. This phenomenon enables a binary value (i.e., 1/0) to represent a relative logic-high/logic-low value of an actuation voltage, and thus the entire electrode controls can be modeled simply. Furthermore, by patterning electrodes to a general 2D array and adopting time-varying actuations, many droplet-based operations (e.g., mixing and cutting) can be well-performed on a 2D array in a *reconfigurable* manner [46].

As schematically presented in **Fig. 7** (a), the general diagram of a 2D EWOD chip contains a patterned electrode array, conduction wires, electrical pads, and a substrate [17], [34], [42], [46]. In order to enable the fabrication of smaller and denser electrodes with high interconnect routing flexibility, a typical two-metal-layer design process of EWOD chips is presented in Refs. [3], [34]. It comprises two metal layers of 2D electrodes patterned in the first layer and conduction wires routed in the second layer, as well as an inter-insulator of silicon dioxide for via holes patterning. Based on this architecture, design model for EWOD chips can be specified to a 2D pin array, in which signal plan and electrical connections between these pins and electrical pads (i.e., signal ports) are established, as illustrated in Fig. 7 (b). As a result, the

^{*1} Note that in chip-level design, routing refers to wire routing, which is different from droplet routing in the fluidic domain.

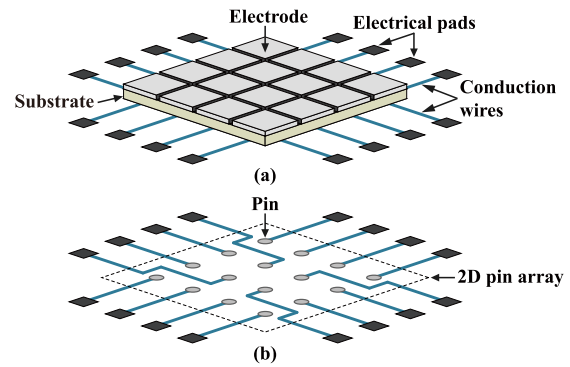


Fig. 7 (1) Schematic view of an EWOD chip. (2) Design model on a 2D pin array.

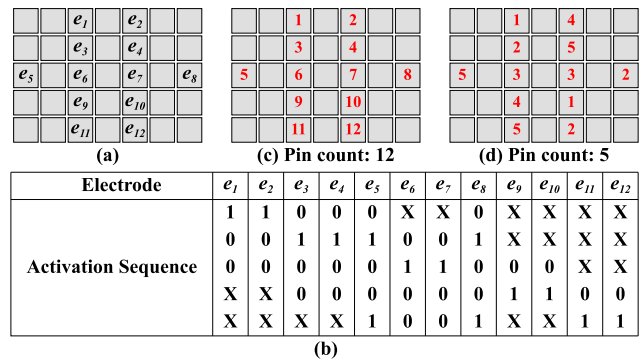


Fig. 8 (a) Electrodes that are used for handling fluidic functions. (b) Scheduled fluidic functions in the form of actuation sequences. (c) Applies the direct-addressing scheme. (d) Applies the broadcast-addressing scheme.

majority of existing efforts can be roughly grouped into two main design steps: 1) electrode addressing and 2) wire routing.

4.2 Electrode Addressing

Electrode addressing is a method whereby electrodes are addressed with control pins to identify input signals. Early EWOD-chip designs relied on *direct addressing* [17], where each electrode is directly addressed with an independent control pin. This addressing scheme maximizes the flexibility of electrode controls. However, since the control pins are actuated by an external controller which supplies a limited number of signal ports, it is infeasible to actuate a large number of control pins especially for high-density electrode array. For example, the controller in a recently developed chip with over 1,000 electrodes for multiplex immunoassay can only actuate 64 control pins [1]. To comply with the limited pin-count supply, *pin-constrained* design of electrode addressing has been introduced as a solution to this problem, which utilizes a limited number of pins to control a large number of electrodes in EWOD chips. A promising solution, *broadcast addressing*, has been presented in Ref. [52]. The droplet-controlling information is stored in the form of electrode actuation sequences, where each bit in a sequence represents a signal status (“1” (actuated), “0” (de-actuated), or “X” (don’t-care)) of the electrode at a specific time step [52]. Note that the don’t-care symbol “X” can be either “1” or “0” which has no impact on scheduled fluidic controls. Examples of an electrode set and their actuation sequences are presented in **Fig. 8** (a) and (b).

Unlike direct addressing, where each electrode is assigned by

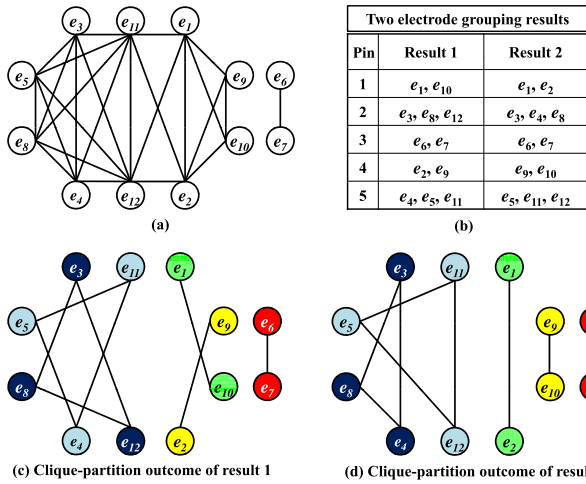


Fig. 9 (a) A compatibility graph G_c derived from Fig. 8(b). (b) Two possible electrode grouping results. (c)–(d) Corresponding clique-partition results of (b).

an independent control pin, broadcast addressing focuses on electrode grouping and control signal merging through the compatibility of actuation sequences. Specifically, each electrode actuation sequence may contain several don't care terms. By carefully replacing these don't care terms with "1" or "0," multiple actuation sequences can be merged to an identical outcome, which is also referred to as the *common compatible sequence* of these electrodes. Therefore, these electrodes can be assigned by the same control pin to receive the same control signal.

Take electrodes e_4 and e_5 in Fig. 8(b) for example. By replacing "X" in the actuation sequence of e_4 with "1," we can merge the actuation sequences of e_4 and e_5 to "01001." Therefore, e_4 and e_5 can be addressed with the same control pin due to their mutually compatible actuation sequences. The example in Fig. 8(c) and (d) demonstrate the direct-addressing and broadcast-addressing outcomes, respectively. Compared with the direct-addressing result in (c), the broadcast-addressing result in (d) significantly reduces the required control pins from 12 to 5. This reduction requires fewer electrical devices and connections to perform the same fluidic functions, thus improving chip reliability as well as reducing fabrication cost [52].

Researchers have utilized the *compatibility graph* to specify the broadcast addressing [52], where the vertex set represents the electrode set and an edge between two electrodes indicates their corresponding activation sequences are compatible. For example, Fig. 9(a) demonstrates a compatibility graph G_c derived from Fig. 8(b). Based on the compatibility graph, the electrode grouping can be mapped to the *clique partition problem*, which is a well-known example of an intractable problem in graph theory. Since each clique represents an electrode group with mutually compatible control signals, we can individually assign each clique with a dedicated control pin. Two feasible electrode grouping results can be shown in Fig. 9(b), with corresponding clique-partition results in Fig. 9(c)–(d). Accordingly, by recognizing a minimum clique partition in the compatibility graph, the required number of control pins can be optimally minimized. However, the general minimum clique partition is known to be NP-hard [18] and thus is computationally expensive.

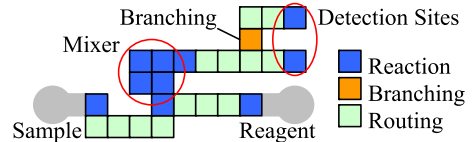


Fig. 10 Categorization of electrodes corresponding to different pin-count demand [30].

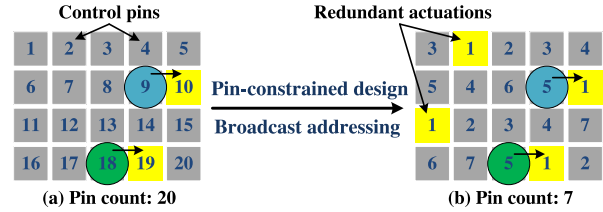


Fig. 11 (a) A direct-addressing result uses two pins (pin 10 and pin 19) to generate two exact actuations for moving the two droplets. (b) A broadcast-addressing result uses one pin (pin 1) to generate two exact actuations, plus two redundant actuations, for moving the two droplets.

To tackle the computational cost, many heuristics have been proposed in Refs. [51], [52], [54]. The work by Ref. [51] proposes an array-partition based method to group the electrode set without introducing unexpected fluidic-level behaviors. The work by Ref. [52] presents a greedy method of iterative clique recognitions with maximum cardinality on the compatibility graph. Recent work by Ref. [54] applies a connect-5 algorithm to group the electrode set with maximum controlling freedom of a single droplet. Moreover, several works further integrates various pin-count saving techniques into fluidic-level synthesis to achieve design convergence, thereby facilitating pin-count reduction effectively [23], [62]. Moreover, a work in Ref. [30] proposes a dedicated pin-count aware design methodology and explores the properties that are favorable for pin-count reduction along the fluidic-level synthesis. It classifies the usage of electrodes into three categories of reaction, branching, and routing corresponding to the design steps of resource binding, placement, and droplet routing as shown in Fig. 10. ILP-based pin-count saving formulations are applied to these three design steps, respectively.

Although broadcast addressing serves as a promising solution to pin-constrained designs, yet the redundant actuations during signal merging have potentially caused a power-consumption problem. For example, in Fig. 11(a), the direct-addressing result needs two exact actuations for moving the two droplets. In Fig. 11(b), after applying the broadcast addressing, the pin count is greatly reduced from 20 to 7. Nevertheless, the addressing result needs two exact actuations, plus two *redundant* actuations, for moving the two droplets. As electrodes are controlled in a series of actuation steps, if control pins are not carefully assigned to electrodes, the addressing result will introduce a great number of redundant actuations. Hence, executing a bioassay may incur a high power-consumption problem which is critical to many battery-driven hand-held applications. Regarding this power-consumption problem, one work has been recently proposed to deal with the power-consumption problem incurred from the pin-constrained design [25]. The work in Ref. [25] formulates the electrode addressing and power saving into an effective minimum-cost maximum-flow network, with a progressive

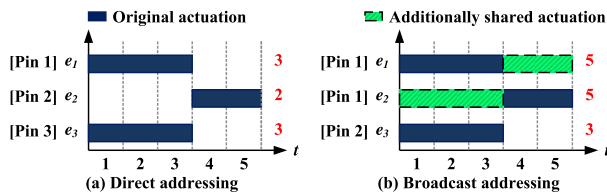


Fig. 12 Broadcast addressing demands more electrode actuations than direct addressing.

electrode-addressing scheme for reducing design complexity.

Furthermore, signal merging in broadcast addressing may also introduce additional (and unnecessary) electrode actuations. Take **Fig. 12** as an example. In (a), the direct-addressing result with 3 pins makes electrodes e_1 , e_2 , and e_3 require 3, 2, and 3 time steps of actuations, respectively. Suppose the control signals of e_1 and e_2 are compatible. After applying the broadcast-addressing method, the pin count can be reduced to 2 pins, as shown in (b). However, this addressing result increases the number of electrode actuations of e_1 and e_2 to 5 time steps, additionally brought from sharing signals with each other. Therefore, if the broadcast-addressing solution is not carefully generated, there is the risk of excessive electrode actuations.

Studies on DMFBs have pointed out that excessive electrode actuations have direct and adverse effect on chip reliability. Two physical phenomena, namely *trapped charge* and *residual charge*, are of the most concern [37], [50]. To tackle both charging problems, a reliability-oriented electrode addressing algorithm has been proposed in Ref. [26], where a matching-based algorithm that formulates the reliability-oriented addressing into a graph-theoretic problem. By further adopting a progressive addressing framework, the entire addressing problem can be efficiently and effectively solved. Our algorithm was modified in Ref. [55] to include the factor of voltage value that is more practical for reliability issue.

4.3 Wire Routing

After electrodes are addressed with control pins, conduction wires must be appropriately routed to establish the correspondence between the control pins (i.e., electrodes with the same pin must be wired together) and the signal pads with a total minimum wirelength. Since signal pads of EWOD chips generally locate outside the component (defined as the 2D pin array) boundary the routing problem that connects these inside terminal pins to outside signal ports is similar to the typical escape routing problem appearing in many VLSI designs [5]. However, in pin-constrained EWOD-chip designs, multiple electrodes may share the same control pin and therefore a single control signal may actuate multi-terminal pins. To realize the electrical connections, multi-terminal pins with the same control signal must be routed together, and then escape to the component boundary. This feature makes the typical escape router, which is based on the connection of two-terminal pins, unsuitable for the EWOD-chip routing problem. However, readily available CAD tools targeting this type of routing problem are still critically lacking.

Regarding the pin-constrained design, a critical problem comes from the interdependence of broadcast addressing and routing.

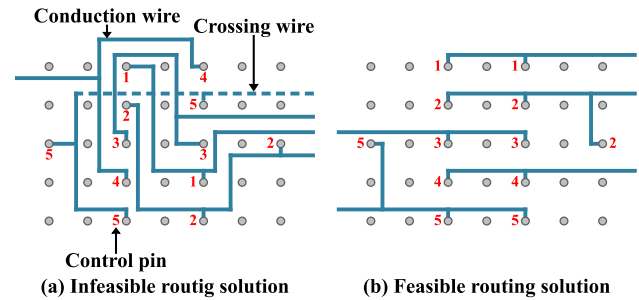


Fig. 13 Consideration of electrode addressing and routing: (a) separately; (b) simultaneously.

Different broadcast-addressing results lead to different wiring connections and this problem occurs even with the same pin count. If broadcast addressing and routing cannot be considered together, the feasibility and quality of the routing solution may be inevitably limited.

For example, **Fig. 13** illustrates two routing solutions under two different design methods that perform the same fluidic controls (the corresponding electrode groups and addressing results can refer to the result 1 and result 2 in Fig. 9 (b), respectively). In (a), the separate consideration of electrode addressing and routing confronts many back detours for pins 3–4, and thus blocks the routing for pin 5. On the other hand, in (b), simultaneous consideration of electrode addressing and routing provides a higher feasibility and quality routing solution in terms of routability and wirelength. In the case of (a), additional post processes such as electrode readdressing and rerouting or even a multi-layer routing structure should be considered. Regarding this, an effective design to low-cost manufacturing of electrical connections cannot be realized [17].

The first work that considers the automated design of EWOD-chip routing is proposed in Ref. [23]. This work simultaneously solves the electrode addressing and routing by adopting a two-stage technique of global routing followed by progressive routing. In global routing, a set of horizontal/vertical global routing tracks is constructed using a maximum-flow formulation. By guiding straight routes on these tracks, the pin count and wirelength can be simultaneously minimized in a global view. Then, the progressive routing iteratively completes the addressing and routing with respect to these tracks using a minimum-cost maximum-flow model, while maintaining a minimum growth of pin count and wirelength between successive iterations.

However, the wire routing problem becomes more critical than ever for modern EWOD-chip designs which need to consider several routing obstacles incurred from permanently embedded devices for specific fluidic protocols [14]. For example, a DNA sequencing chip may embed several electrophoresis devices for fast and accurate sample isolation, DNA amplification protocols require on-chip sensors to monitor the temperature variation for each amplification cycle, immunoassay protocols require on-chip magnets to capture antibodies, protein or DNA analysis require on-chip electrophoresis equipments to separate and identify individual components (i.e., ions and particles) in reaction products, etc [15]. As these devices are independent from EWOD actuations, they are typically regarded as on-chip obstacles. During

the EWOD-chip routing, conduction wires should avoid routing through these obstacles, thereby increasing the problem complexity. To solve this problem, an integer-linear-programming (ILP)-based obstacle-avoiding routing algorithm is proposed [8]. Based on effective ILP formulation as well as efficient routing framework, simultaneous consideration avoids wiring across the obstacle, thereby providing a higher solution feasibility and quality in terms of routability and wirelength.

5. Cyberphysical Integration

For biomedical applications such as clinical diagnostics, it is necessary to ensure the accuracy of on-chip fluidic operations. The accuracy of fluid-handling operations can be monitored by examining parameters such as the volume and concentration of product droplets. If an error occurs during the execution of the bioassay, for instance, the volume of an intermediate product droplet exceeds the normal value, the assay outcomes can be incorrect and the whole experiment needs to be re-executed. Therefore, it is important to detect such errors as early as possible and re-execute the corresponding fluid-handling operations to obtain correct bioassay outcomes. Considering this issue, a control-path based design is integrated to the architectural-level synthesis of DMFBs [59]. In Ref. [59], they first calculate the possibilities of errors for each operation via an error-propagation estimates, and then insert a check point consisting of a storing operation and an error detection to the sequencing graph, as shown in Fig. 14. A simulated-annealing (SA) method is also proposed to optimize the execution time used for error recovery.

However, today’s DMFBs suffer from the drawback that there is no feedback to the control software from the underlying hardware platform. Due to the lack of precision that is often inherent in biochemical experiments, errors are likely during droplet manipulation, but error recovery based on the repetition of experiments leads to wastage of expensive reagents and hard-to-prepare samples. Thus, by exploiting recent advances in the integration of sensing system in a DMFB, a “physical-aware” system reconfiguration technique that uses sensor data at intermediate checkpoints to dynamically reconfigure the biochip can be implemented. A cyberphysical re-synthesis technique is used to recompute electrode-actuation sequences, thereby deriving new schedules, module placement, and droplet routing pathways, with minimum impact on the time-to-response [32], [33].

5.1 Overview of Cyberphysical Biochips

In this section, we investigate the idea of cyberphysical microfluidics – a transformative approach towards achieving closed-

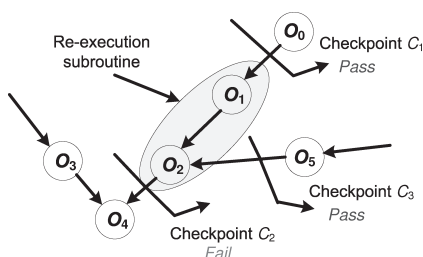


Fig. 14 Checkpoint insertion and re-execution subroutine [59].

loop and sensor feedback-driven biochip operation under program control. With the availability of sensing system for biochips, “physical-aware” control software becomes feasible. By “physical-aware,” we refer to the fact that the software can receive information about the outcome (error-free/erroneous) of fluid-handling operations based on feedback from the sensing system. Depending on sensor feedback, the control software can appropriately reconfigure the microfluidic biochip. In this way, the various steps in the bioassay are executed based upon real-time sensing of intermediate results.

Figure 15 depicts each component of a cyberphysical system on the microfluidic platform. The control software sends a control signal to the microfluidic biochip, and the on-chip sensing system monitors the outcomes of fluidic operations. The outcomes are compared with the “expected values,” i.e., the pre-determined thresholds. If the results of the comparison indicate that an error has occurred, the control software receives a “repeat request,” and the corresponding operation in which the error occurred can be executed again, thereby correcting the error.

5.2 Sensing Systems

As described in Refs. [14], [41], CCD cameras can be used in experiments to view the top sides of droplets simultaneously. An example of the CCD monitoring system is shown in Fig. 16.

Based on images captured by the CCD camera, droplets can be automatically located by the control software. The procedure of automatically searching for droplets can be described as a “template matching” problem. Here a pattern can be represented as the image of a “typical” droplet. During the matching process, we move the template image to all possible positions in the image of the entire array and crop a sub-image that has the same size as the template image. Then the control software computes the correlation index, which indicates the similarity between the template and the “cropped image.” This process is shown in Fig. 17 (a) and the correlation factor is calculated on a pixel-by-pixel basis.

In the control software, all images are stored in grayscale form, which can be encoded as matrices or vectors. Suppose the template image is represented in a 1-D array: $\vec{x} = (x_1, x_2, \dots, x_N)$. Here x_i represents the grayscale level of a pixel and N is the total

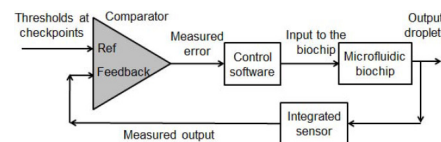


Fig. 15 The schematic of the cyberphysical digital microfluidic system.

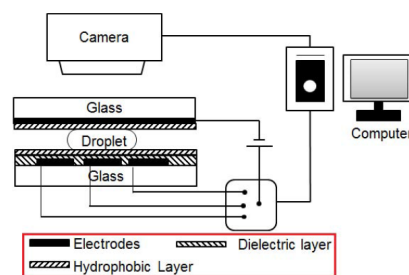


Fig. 16 Illustration of a digital microfluidics-based image processing system [41].

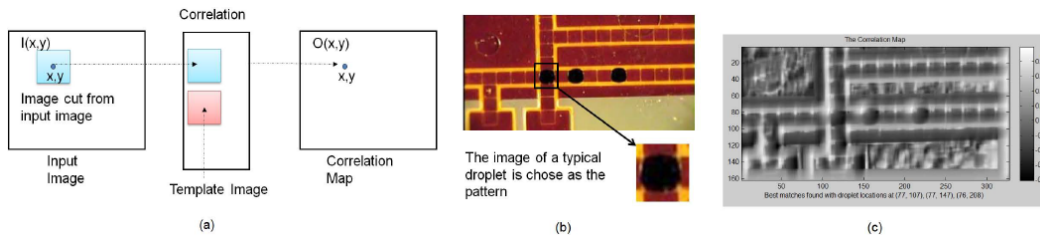


Fig. 17 (a) The matching process moves the template image to all possible positions in a larger source image and computes a numerical index that indicates how well the template matches the sub-image in that position; (b) the image of the whole array [61] and the pattern we selected; (c) the correlation map between image of the whole array and the pattern. The positions of droplets can be determined by finding κ maximum elements (κ is the number of droplets on the chip) in the correlation map.

number of pixels in the template image. Similarly, the cropped sub-image to be compared with the template image can be written as $\vec{y} = (y_1, y_2, \dots, y_N)$. Thus the correlation factor between these two images is defined as:

$$cor = \frac{\sum_{i=1}^N (x_i - \bar{x}) \cdot (y_i - \bar{y})}{\sqrt{\sum_{i=1}^N (x_i - \bar{x})^2 \cdot \sum_{i=1}^N (y_i - \bar{y})^2}}$$

where \bar{x} and \bar{y} are the average gray level in the template image and cropped sub-image, respectively. The range of correlation factor cor is a real number between -1 and $+1$. According to the definition of correlation, a larger value represents a stronger relationship between two images.

After deriving the correlation factors for all possible positions in the image for the complete biochip, we obtain the correlation map between the template and the original input image. Suppose there are κ droplets on the biochip. By searching for the largest κ correlation factors in the correlation map, the locations of droplets can be determined. An example is shown in Fig. 17 (b) and (c) [61]. Part (b) shows the original input image of the whole chip and the pattern image, and (c) is the correlation map, where the best matching locations, i.e. the coordinations of droplets derived by the control software are $(77, 107)$, $(77, 147)$ and $(76, 208)$. Thus the control software automatically locates the droplets, and it can further analyze the sizes and colors of droplets according to the image. In this manner, the volumes and concentrations of droplets can be acquired after processing the image taken by the CCD camera.

Instead of searching for droplets in the complete image, we use imaging to check whether the droplets have been moved to the expected positions. This is implemented using the following steps:

First, we do some calibration before the experiment. We choose a large number of sub-images with (or without) droplets, and calculate their correlation with the template. Based on this calculation, we find an appropriate threshold for the correlation index (C_{th}): if the correlation is larger than C_{th} , we conclude that there is a droplet in the cropped sub-image; otherwise, there is no droplet in the sub-image. When the bioassay is running, we only need to crop the sub-images near the expected positions of droplets, and calculate their corresponding correlation indices to determine the absence/presence of droplets.

The advantages of the CCD camera-based sensing system are: (i) the detection of errors immediately after they occur and (ii) the identification of the precise locations of the errors. A disadvantage of this system is that extra instruments, such as CCD cameras, are required to observe the cyberphysical system.

The second sensing scheme is based on integrated optical detectors, as proposed in Refs. [13], [27]. The quality of an intermediate product in a digital microfluidic biochip can be determined by examining the concentration of the product in the droplets through fluorescence Refs. [13], [27]. When a fluorophore tag is attached to a droplet, different product concentrations lead to the emission of light different wavelengths (i.e., different colors). This difference in color can be detected by sensors that convert the received light into electrical current or a voltage signal [13]. In recent work, integrated photodetectors have been introduced on the microfluidic array [13], [27]. For example, in Ref. [27], a detection system was integrated with the digital microfluidic array. It consists of a light-emitting diode (LED) and a photodiode which functions as light-to-voltage converter. The concentration of products on the array can be measured by the absorbance of the droplets using a kinetic rate method. As another example, thin film InGaAs photodetectors can be bonded onto a glass platform, coated with Teflon AF, and then integrated into the digital microfluidic system.

5.3 Interfaces between Biochip and Control Software

We next describe the cyberphysical coupling between the control software and the hardware of the microfluidic platform. There are two interfaces needed for cyberphysical coupling. The first interface converts the output signals from the sensing system to the inputs of the desktop computer that the control software can interpret. The second interface converts the output data generated by the control software to voltage signals that can be directly applied to the electrodes of the biochip.

As described in Ref. [49], biochip synthesis includes resource binding and scheduling, which specifies the start and stop times of fluidic operations. The synthesis results (control software) need to be mapped to a sequence of electrode actuation vectors consisting of “0,” “1,” and “F” (floating). A programmable logic controller (PLC) is used as the interface between the output of the control software (“controller”) and the control pins of the biochip.

During bioassay execution, the PLC reads the electrode actuation sequences stored in memory and applies the appropriate se-

quence of voltages to the output pins. When the PLC generates output voltages based on sequences in its memory, corresponding activation voltages are applied to the electrodes of the biochip. The quality of an intermediate product in a digital microfluidic biochip can be determined by examining the product concentration in droplets through fluorescence [16], [39]. When a fluorophore tag is attached to a droplet, different product concentrations lead to emitted light of different wavelengths (i.e., different colors). This difference in color can be detected by the sensing system that converts the received analog signals into electrical current or voltage [14]. Recent advances in the integration of a multiplicity of such miniaturized sensors provide an important motivation for the cyberphysical hardware/software co-design approach [32], [33].

6. Future Design Challenges

To meet the challenges of increasing design complexity, current CAD tools generally conduct a two-stage based design flow of fluidic-level synthesis followed by chip-level design to optimize fluidic behaviors and chip architecture separately. Nevertheless, existing fluidic-chip design gap will become even wider with a rapid escalation in the number of assay operations incorporated into a single DMFB. As more and more large-scale assay protocols are delivered in current emerging marketplace, this problem may potentially restrict the effectiveness and feasibility of the entire DMFB realization and thus needs to be solved quickly. Currently, only one fluidic-chip codesign methodology for DMFBs to effectively bridge the fluidicchip design gap is proposed [9]. This work provides a comprehensive integration throughout fluidic-operation scheduling, chip layout generation, control pin assignment, and wiring solution to achieve higher design performance and feasibility. However, future design challenges lie in the incorporation of chip reliability into the codesign flow of DMFB.

One significant problem is the reliability problem incurred from pin-constrained designs. Control-pin/-signal sharing might introduce additional and unnecessary electrode actuations, which has the potential to make an electrode confront excessive actuations in case of a naive design. Studies on EWOD chips have reported this kind of problem accelerates the extent of trapping charge, leading to a permanent degradation of dielectric layer [12], [28], [50]. This scenario inevitably impedes complete and correct fluidic controls and therefore degrades the chip reliability. Thus, it becomes desirable and crucial to strike a balance between control-pin sharing and reliability preservation when the chip size and assay functionality grow, especially under the circumstance of pin-constrained design and cyberphysical integration.

Optimization across energy domains also needs to be investigated. Such optimization problems that span several energy domains (e.g., electrical, circuit, fluidic, and thermal domains) appear to be extremely difficult due to the further involvements of energy-related constraints or objectives. For example, in pin-constrained design, we should limit the fanout of a single control pin to avoid overly charge sharing, which might cause problems such as high power dissipation and trapped charge. Moreover, thermal-aware signal planning is also important for the preven-

tion of fluidics from overheating in some area that has congested electrical connections.

Biochip operation execution is in the order of seconds, whereas specialized heuristics for the synthesis problems can potentially obtain good results in milliseconds [40]. An interesting possibility in this context is to perform the synthesis online, while the biochemical application is running, and not offline, as it has been done so far. Such an online approach has the advantage of adaptivity, to faults in the architecture or variations in the operation execution. In addition, it opens up the possibility of fully portable point-of-care devices. Although no research has been done so far in this area, recent research [4], [59] has shown how an implementation can react to faults by switching online to recovery schedules pre-synthesized offline.

7. Conclusions

In this paper, we have provided a survey on recent research in the design and optimization of DMFBs. We show how CAD tools are involved to automate the design of DMFBs. Several optimization problems appearing in the design stages, fluidic-level synthesis, chip-level design, and cyberphysical integration, are also presented. In addition, we have pointed out a set of open problems and design challenges that remain to be tackled in the future. The authors believe this paper will spark more research interests being devoted into the developments of CAD tools for DMFBs, which are expected to pave the way for the deployment and use of biochips in the emerging marketplace.

Acknowledgments This work was supported in part by the Taiwan National Science Council under grant no. NSC 101-2220-E-006-016, 101-2628-E-006-018-MY3, and 102-2221-E-006-287-MY3 and the Ministry of Education, Taiwan, R.O.C. under the NCKU Aim for the Top University Project Promoting Academic Excellence & Developing World Class Research Centers.

References

- [1] Advanced Liquid Logic, Inc., available from (<http://www.liquid-logic.com>).
- [2] Frost & Sullivan, available from (<http://www.frost.com>).
- [3] Microfluidic Lab., Duke University, available from (<http://microfluidics.ee.duke.edu/>).
- [4] Alistar, M., Maftai, E., Pop, P. and Madsen, J.: Synthesis of biochemical applications on digital microfluidic biochips with operation variability, *Proc. DTIP*, pp.350–357 (2010).
- [5] Alpert, C.J., Mehta, D.P. and Sapatnekar, S.S.: *Handbook of Algorithms for Physical Design Automation*, CRC Press (2009).
- [6] Chakrabarty, K.: Towards fault-tolerant digital microfluidic lab-on-chip: defects, fault modeling, testing, and reconfiguration, *Proc. IEEE ICBCS*, pp.329–332 (2008).
- [7] Chakrabarty, K.: Design automation and test solutions for digital microfluidic biochips, *IEEE Trans. CAS I*, Vol.57, pp.4–17 (2010).
- [8] Chang, J.-W., Huang, T.-W. and Ho, T.-Y.: An ILP-based Obstacle-Avoiding Routing Algorithm for Pin-Constrained EWOD Chips, *Proc. IEEE/ACM ASPDAC*, pp.67–72 (2012).
- [9] Chang, J.-W., Yeh, S.-H., Huang, T.-W. and Ho, T.-Y.: Integrated Fluidic-Chip Co-Design Methodology for Digital Microfluidic Biochips, *IEEE Trans. CAD*, Vol.32, No.2, pp.216–227 (2013).
- [10] Chen, Y.-H., Hsu, C.-L., Tsai, L.-C., Huang, T.-W. and Ho, T.-Y.: A Reliability-Oriented Placement Algorithm for Reconfigurable Digital Microfluidic Biochips Using 3D Deferred Decision Making Technique, *IEEE Trans. CAD*, Vol.32, No.8, pp.1151–1162 (2013).
- [11] Cho, M. and Pan, D.Z.: A high-performance droplet routing algorithm for digital microfluidic biochips, *IEEE Trans. CAD*, Vol.27, No.10, pp.1714–1724 (2008).

- [12] Drygiannakis, A.I., Papathanasiou, A.G. and Boudouvis, A.G.: On the connection between dielectric breakdown strength, trapping of charge, and contact angle saturation in electrowetting, *ACS J. Langmuir*, No.25, pp.147–152 (2009).
- [13] Evans, R., Luan, L., Jokerst, N.M. and Fair, R.B.: Optical detection heterogeneously integrated with a coplanar digital microfluidic lab-on-a-chip platform, *Proc. IEEE Sensors*, pp.423–426 (2007).
- [14] Fair, R.B.: Digital microfluidics: Is a true lab-on-a-chip possible?, *Microfluidics and Nanofluidics*, Vol.3, pp.245–281 (2007).
- [15] Fair, R.B., Khlystov, A., Tailor, T.D., Ivanov, V., Evans, R.D., Griffin, P.B., Vijay, S., Pamula, V.K., Pollack, M.G. and Zhou, J.: Chemical and Biological Applications of Digital-Microfluidic Devices, *IEEE Design and Test*, Vol.24, pp.20–24 (2007).
- [16] Furtado, A. and Henry, R.: Measurement of green fluorescent protein concentration in single cells by image analysis, *Analytical Biochemistry*, pp.84–92 (Nov. 2002).
- [17] Gong, J. and Kim, C.J.: Direct-referencing two-dimensional-array digital microfluidics using multilayer printed circuit board, *IEEE J. MEMS*, No.2, pp.257–264 (2008).
- [18] Gross, J.L. and Yellen, J.: Graph Theory and Its Application, CRC Press, FL (1999).
- [19] Ho, T.-Y., Zeng, J. and Chakrabarty, K.: Digital microfluidic biochips: A vision for functional diversity and more than Moore, *Proc. IEEE/ACM ICCAD*, pp.578–585 (2010).
- [20] Ho, T.-Y., Pop, P. and Chakrabarty, K.: Microfluidic biochips: Recent research and emerging challenges, *Proc. IEEE/ACM CODES+ISSS*, pp.335–343 (2011).
- [21] Huang, T.-W. and Ho, T.-Y.: A fast routability- and performance-driven droplet routing algorithm for digital microfluidic biochips, *Proc. IEEE ICCD*, pp.445–450 (2009).
- [22] Huang, T.-W., Lin, C.-H. and Ho, T.-Y.: A contamination aware droplet routing algorithm for digital microfluidic biochips, *Proc. IEEE/ACM ICCAD*, pp.151–156 (2009).
- [23] Huang, T.-W. and Ho, T.-Y.: A two-stage ILP-based droplet routing for pin-constrained digital microfluidic biochips, *Proc. ACM ISPD*, pp.201–208 (2010).
- [24] Huang, T.-W., Yeh, S.-Y. and Ho, T.-Y.: A network-flow based pin-count aware routing algorithm for broadcast electrode-addressing EWOD chips, *Proc. IEEE/ACM ICCAD*, pp.425–431 (2010).
- [25] Huang, T.-W., Su, H.-Y. and Ho, T.-Y.: Progressive network-flow based power-aware broadcast addressing for pin-constrained digital microfluidic biochips, *Proc. ACM/IEEE DAC*, pp.741–746 (2011).
- [26] Huang, T.-W., Ho, T.-Y. and Chakrabarty, K.: Reliability-Oriented Broadcast Electrode-Addressing for Pin-Constrained Digital Microfluidic Biochips, *Proc. IEEE/ACM ICCAD*, pp.448–455 (2011).
- [27] Jokerst, N., Luan, L., Palit, S., Royal, M., Dhar, S., Brooke, M. and Tyler II, T.: Progress in chip-scale photonic sensing, *IEEE Trans. BioCAS*, Vol.3, pp.202–211 (2009).
- [28] Kerber, A., Cartier, F., Degraeve, R., Roussel, P.J., Pantisano, L., Kauerauf, T., Groeseneken, G., Maes, H.E. and Schwalke, U.: Charge trapping and dielectric reliability of SiO₂-Al₂O₃ gate stacks with TiN electrodes, *IEEE Trans. Electron Devices*, No.50, pp.1261–1269 (2003).
- [29] Chakrabarty, K., Fair, R.B. and Zeng, J.: Design tools for digital microfluidic biochips: Towards functional diversification and more than Moore, *IEEE Trans. CAD*, Vol.29, pp.1001–1017 (July 2010).
- [30] Lin, C.C.-Y. and Chang, Y.-W.: ILP-based pin-count aware design methodology for microfluidic biochips, *Proc. ACM/IEEE DAC*, pp.258–263 (2009).
- [31] Lin, C.C.-Y. and Chang, Y.-W.: Cross-contamination aware design methodology for pin-constrained digital microfluidic biochips, *Proc. ACM/IEEE DAC* (2010).
- [32] Luo, Y., Chakrabarty, K. and Ho, T.-Y.: Dictionary-Based Error Recovery in Cyberphysical Digital-Microfluidic Biochips, *Proc. IEEE/ACM ICCAD*, pp.369–376 (2012).
- [33] Luo, Y., Chakrabarty, K. and Ho, T.-Y.: Error Recovery in Cyberphysical Digital-Microfluidic Biochips, *IEEE Trans. CAD*, Vol.32, No.1, pp.59–72 (2013).
- [34] Lin, Y.-Y., Evans, R.D., Welch, E., Hsu, B.N., Madison, A.C. and Fair, R.B.: Low Voltage Electrowetting-on-Dielectric Platform using Multi-Layer Insulators, *Sensors and Actuators B: Chemical*, pp.465–470 (2010).
- [35] Maftai, E., Pop, P. and Madsen, J.: Tabu search-based synthesis of dynamically reconfigurable digital microfluidic biochips, *Proc. ACM CASES*, pp.195–203 (2009).
- [36] Maftai, E., Pop, P. and Madsen, J.: Routing-based synthesis of digital microfluidic biochips, *Design Autom. for Emb. Sys.*, Vol.16, No.1, pp.19–44 (2012).
- [37] Park, J.K., Lee, S.J. and Kang, K.H.: Fast and reliable droplet transport on single-plate electrowetting on dielectrics using nonfloating switching method, *J. Biomicrofluidics*, No.4 (2010).
- [38] Pollack, M.G., Shenderov, A.D. and Fair, R.B.: Electrowetting-based actuation of droplets for integrated microfluidics, *LOC*, pp.96–101 (2002).
- [39] Rodriguez-Cruz, S., Khoury, J. and Parks, J.: Protein fluorescence measurements within electrospray droplets, *Journal of the American Society for Mass Spectrometry*, pp.716–725 (2001).
- [40] Sjogreen, C.E.: Synthesis of Biochemical Applications with Operation Variability on Digital Microfluidic Biochips, Bachelor Thesis, Technical University of Denmark (2011).
- [41] Shin, Y. and Lee, J.: Machine vision for digital microfluidics, *Review of Scientific Instruments*, No.014302, pp.1–8 (2010).
- [42] Song, J.H., Evans, R., Lin, Y.Y., Hsu, B.N. and Fair, R.B.: A scaling model for electrowetting-on-dielectric microfluidic actuators, *Microfluidics and Nanofluidics*, pp.75–89 (2009).
- [43] Su, F. and Chakrabarty, K.: Architectural-level synthesis of digital microfluidics-based biochips, *Proc. IEEE/ACM ICCAD*, pp.223–228 (2004).
- [44] Su, F. and Chakrabarty, K.: Unified high-level synthesis and module placement for defect-tolerant microfluidic biochips, *Proc. ACM/IEEE DAC*, pp.825–830 (2005).
- [45] Su, F. and Chakrabarty, K.: Reconfiguration techniques for digital microfluidic biochips, *Proc. DTIP*, pp.143–148 (2005).
- [46] Su, F., Chakrabarty, K. and Fair, R.B.: Microfluidics based biochips: Technology issues, implementation platforms, and design-automation challenges, *IEEE Trans. CAD*, pp.211–223 (2006).
- [47] Su, F. and Chakrabarty, K.: Module placement for fault-tolerant microfluidics-based biochips, *ACM TODAES*, Vol.11, pp.682–710 (2006).
- [48] Su, F., Hwang, W. and Chakrabarty, K.: Droplet routing in the synthesis of digital microfluidic biochips, *Proc. IEEE/ACM DATE*, pp.1–6 (2006).
- [49] Su, F. and Chakrabarty, K.: High-level synthesis of digital microfluidic biochips, *ACM JETC*, Vol.3 (2008).
- [50] Verheijen, H.J.J. and Prins, M.W.J.: Reversible electrowetting and trapping of charge: Model and experiments, *ACS J. Langmuir*, No.15, pp.6616–6620 (1999).
- [51] Xu, T. and Chakrabarty, K.: Droplet-trace-based array partitioning and a pin assignment algorithm for the automated design of digital microfluidic biochips, *Proc. ACM CODES+ISSS*, pp.112–117 (2006).
- [52] Xu, T. and Chakrabarty, K.: Broadcast electrode-addressing for pin-constrained multi-functional digital microfluidic biochips, *Proc. ACM/IEEE DAC*, pp.173–178 (2008).
- [53] Xu, T. and Chakrabarty, K.: Integrated droplet routing and defect tolerance in the synthesis of digital microfluidic biochips, *ACM JETC*, Vol.4, No.3 (2008).
- [54] Xu, T., Chakrabarty, K. and Pamula, V.K.: Defect-tolerant design and optimization of a digital microfluidic biochip for protein crystallization, *IEEE Trans. CAD* (2010).
- [55] Yeh, S.-H., Chang, J.-W., Huang, T.-W. and Ho, T.-Y.: Voltage-Aware Chip-Level Design for Reliability-Driven Pin-Constrained EWOD Chips, *Proc. IEEE/ACM ICCAD*, pp.353–360 (2012).
- [56] Yuh, P.-H., Yang, C.-L. and Chang, Y.-W.: Placement of defect-tolerant digital microfluidic biochips using the T-tree formulation, *ACM JETC*, Vol.3, No.3 (2007).
- [57] Yuh, P.-H., Yang, C.-L. and Chang, Y.-W.: BioRoute: A network flow based routing algorithm for the synthesis of digital microfluidic biochips, *IEEE Trans. CAD*, Vol.27, No.11, pp.1928–1941 (2008).
- [58] Zhao, Y. and Chakrabarty, K.: Cross-contamination avoidance for droplet routing in digital micro fluidic biochips, *Proc. IEEE/ACM DATE*, pp.1290–1295 (2009).
- [59] Zhao, Y., Xu, T. and Chakrabarty, K.: Control-path design and error recovery in digital microfluidic lab-on-chip, *ACM JETC*, Vol.3, No.11 (2010).
- [60] Zhao, Y., Xu, T. and Chakrabarty, K.: Synchronization of washing operations with droplet routing for cross-contamination avoidance in digital microfluidic biochips, *Proc. ACM/IEEE DAC*, pp.635–640 (2010).
- [61] Zhao, Y. and Chakrabarty, K.: Digital microfluidic logic gates and their application to built-in self-test of lab-on-chip, *IEEE Trans. BioCAS*, Vol.4, pp.250–262 (2010).
- [62] Zhao, Y. and Chakrabarty, K.: Co-optimization of droplet routing and pin assignment in disposable digital microfluidic biochips, *Proc. ACM ISPD*, pp.69–76 (2011).



Tsung-Yi Ho received his Ph.D. degree in Electrical Engineering from National Taiwan University, Taipei, Taiwan, R.O.C., in 2005. Since 2007, he has been with the Department of Computer Science and Information Engineering, National Cheng Kung University, Tainan, Taiwan, R.O.C., where he is currently an Associate Professor.

His research interests include design automation for microfluidic biochips and nanometer integrated circuits. He has published several papers in top journals and conferences such as IEEE TCAD, ACM TODAES, ACM/IEEE DAC, IEEE/ACM ICCAD, ACM ISPD, and etc. He was the recipient of many research awards, such as Dr. Wu Ta-You Memorial Award of National Science Council (NSC) of Taiwan (the most prestigious award from NSC for junior researchers), Distinguished Young Scholar Award of Taiwan IC Design Society, Outstanding Young Electrical Engineer Award of Chinese Institute of Electrical Engineering, K.T. Li Research Award of Delta Electronics, ACM Taipei Chapter Young Researcher Award, IEEE Tainan Chapter Gold Member Award, the Invitational Fellowship of the Japan Society for the Promotion of Science (JSPS), Japan, and the Humboldt Research Fellowship from the Alexander von Humboldt Foundation, Germany. Currently, he serves as a Distinguished Visitor of the IEEE Computer Society, the Chair of IEEE Computer Society Tainan Chapter, and an Associate Editor of ACM Journal on Emerging Technologies in Computing Systems and IEEE Transactions on Computer-Aided Design of Integrated Circuits and Systems. He is a senior member of IEEE.

(Invited by Editor-in-Chief: *Hiroyuki Tomiyama*)